

# The NLTE formation of neutral-boron lines in cool stars

Dan Kiselman<sup>1,2</sup> and Mats Carlsson<sup>3</sup>

<sup>1</sup> NORDITA, Blegdamsvej 17, DK-2100 Copenhagen, Denmark

<sup>2</sup> The Royal Swedish Academy of Sciences, Stockholm Observatory, S-133 36 Saltsjöbaden, Sweden

<sup>3</sup> Institute of Theoretical Astrophysics, University of Oslo, Box 1029, Blindern, N-0315 Oslo, Norway

Received 4 October 1995 / Accepted 21 December 1995

**Abstract.** We study the formation of B I lines in a grid of cool stellar model atmospheres without the assumption of local thermodynamic equilibrium (LTE). The non-LTE modelling includes the effect of other lines blending with the B I resonance lines. Except for the cases where the B I lines are very strong, the departures from LTE relevant for the resonance lines can be described as an overionisation effect and an optical-pumping effect. This causes the lines to be weaker than in LTE so that an abundance analysis assuming LTE will underestimate stellar boron abundances. We present non-LTE abundance corrections useful to improve on abundances derived from the B I 250 nm and 209 nm lines under the LTE assumption. Application of the results on literature data indicates that the B/Fe ratio in metal-poor stars is constant.

**Key words:** Line: formation, Stars: abundances, Stars: atmospheres, Galaxy: abundances, Boron

## 1. Introduction

The Hubble Space Telescope has made it possible to derive boron abundances for cool stars by observation of the B I resonance doublet at 250 nm. (Duncan et al. 1992; Lemke et al. 1993; Edvardsson et al. 1994; Duncan et al. 1995; more publications will certainly follow.) These abundances, for stars of different ages and in different evolutionary stages, can give important clues to the origin of the light elements and to stellar evolution. It is important that the abundances derived are correct, so the validity of the stellar abundance analyst's standard approximations of plane-parallel stellar atmospheres with line formation in local thermodynamic equilibrium (LTE) must be investigated.

*Send offprint requests to:* Dan Kiselman (Stockholm Observatory)

Kiselman (1994) investigated the statistical equilibrium of neutral boron in three solar-type atmospheric models and found significant departures from LTE in stars hotter or more metal-poor than the Sun. The most important process causing these departures was found to be the pumping in the ultraviolet resonance lines that gives rise to line source functions exceeding the local Planckian value and to overionisation. The effects on derived abundances are significant when it comes to interpretation of observations of metal-poor halo stars (Edvardsson et al. 1994).

The aim of this paper is to investigate the formation of B I lines in cool stars and to provide non-LTE abundance corrections in a form that is convenient to use for general observers. To this end we have studied the B I lines in a grid of model atmospheres and for a range of boron abundances. We will first present the techniques used, then discuss the line-formation circumstances and their dependence on atmospheric parameters, and finally present abundance corrections that are of practical use for abundance analysts using LTE spectral synthesis. The discussion concentrates on the lines which are of observational interest, the least blended in each of the 250 nm and 209 nm doublets, that is  $\lambda_{\text{vac}} = 249.75$  nm and  $\lambda_{\text{vac}} = 209.02$  nm ( $\lambda_{\text{air}} = 249.68$  nm and  $\lambda_{\text{air}} = 208.96$  nm), all wavelengths from Johansson et al. 1993). These lines will be referred to as the 250 nm and the 209 nm lines. The 209 nm doublet holds some promise in being useful for determining boron isotopic ratios (Johansson et al. 1993), but no detailed observational analysis of these lines have yet been published.

## 2. Methods

### 2.1. Conventions

We express elemental abundances on the customary scale where the abundance

$$A_X = \lg N(X)/N(H) + 12,$$

with  $\lg$  being the logarithm, base 10.

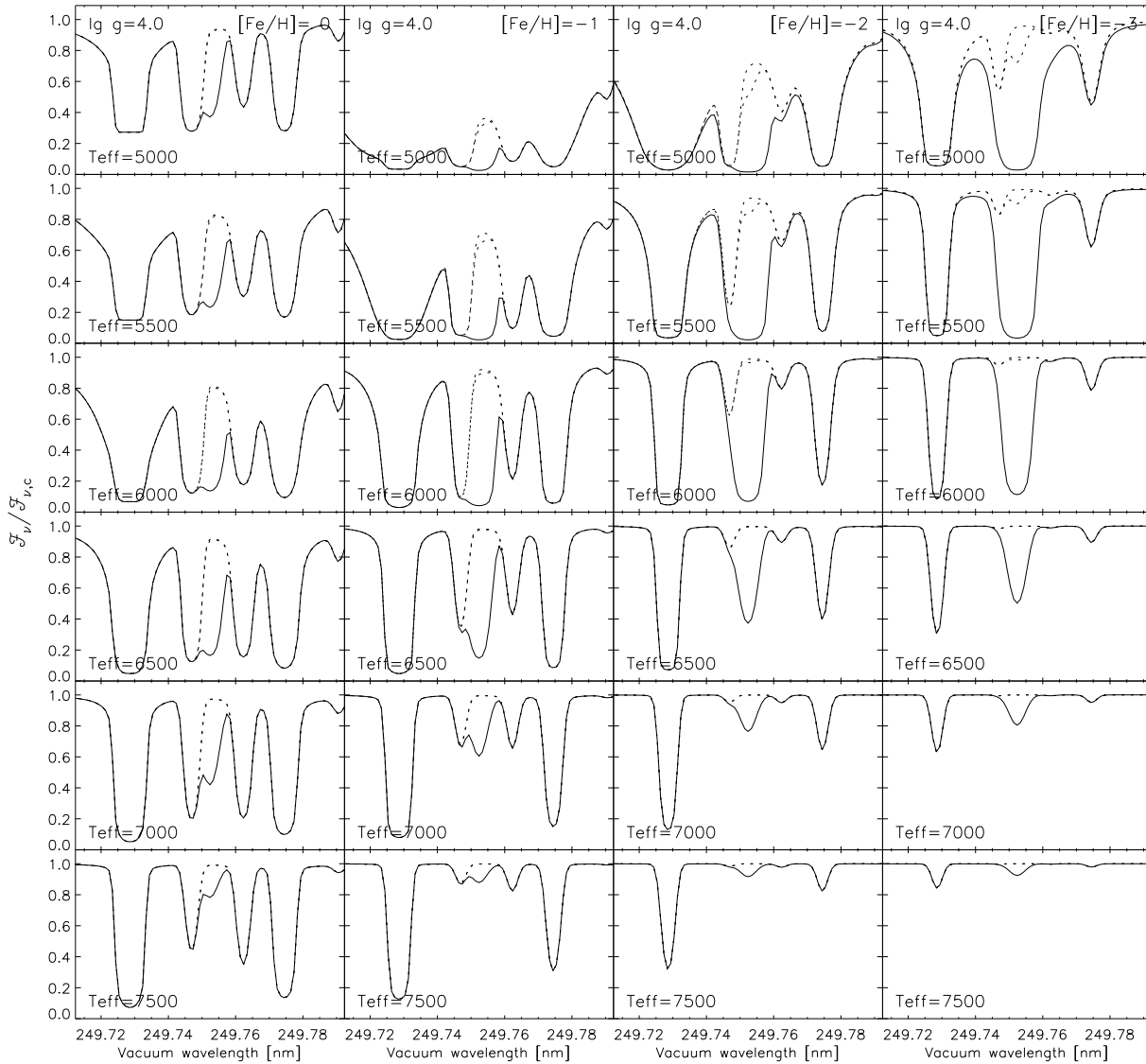


**Fig. 1.** Synthetic flux spectra for the region around B I 249.75 nm, the section of the grid with  $\lg g = 4.0$ . The spectra have been normalised to the continuum level as computed without lines. No instrumental, macro-turbulent, or rotational broadening have been applied. Solid curve:  $A_B = 2.6$ . Dotted curves:  $A_B = 0.0$  and no boron

Overall metallicity is given relative to solar as

$$[\text{Fe}/\text{H}] = \lg \frac{N(\text{Fe})}{N(\text{H})} - \lg \frac{N(\text{Fe})}{N(\text{H})}_{\odot}.$$

To comply with common usage in stellar atmosphere work, the logarithm of the surface gravity,  $\lg g$  is given with  $g$  in cgs units.

Quantities denoted with an asterisk, e.g.  $N^*$ , are LTE values.

## 2.2. Model atmospheres

The model atmospheres were produced using the code OS-MARCS of Edvardsson et al. (1993) which is an extended version of the MARCS program (Gustafsson et al. 1975).

This code includes a great number of spectral lines in the blue and ultraviolet by means of opacity sampling. The line data are from the Kurucz compilation (e.g. Kurucz 1991) and it has been claimed (Kurucz 1991; Edvardsson et al. 1993) that inclusion of these opacities solves the so-called “missing-opacity problem” for the blue and ultraviolet parts of the solar spectrum. It has, however, been questioned (Bell et al. 1994, see also Gustafsson 1995 and Bell & Tripicco 1995) whether the adding of these line opacities really solve the problem in the right way, i.e. the resulting models may reproduce the observed flux spectrum well at low resolution but badly at high resolution. If this is the case, systematic errors may appear in comparisons of different stars. We consider, however, these models

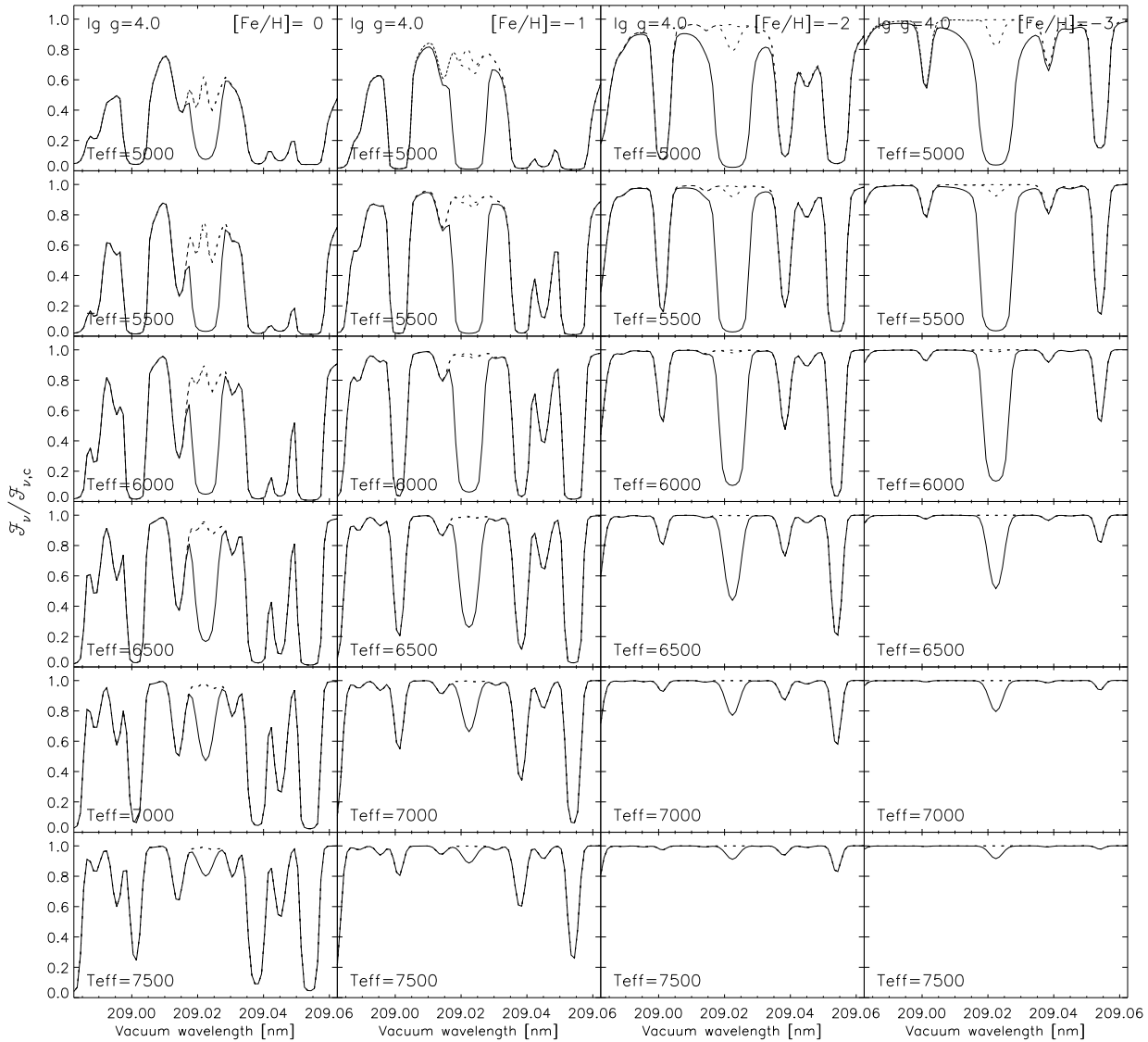


**Fig. 2.** Synthetic flux spectra for the region around B I 209 nm, same treatment as in Fig. 1. Solid curve:  $A_B = 2.6$ . Dotted curves:  $A_B = 0.0$  and no boron

as the best choice, since they apparently are successful in reproducing the ultraviolet fluxes of solar-type stars of different metallicities (Edvardsson et al. 1993, Duncan et al. 1992), something which is crucial for the current study.

The radiation-field values for different depths and wavelengths that are produced by the atmosphere code are saved and used in the non-LTE spectral modelling for the calculation of the fixed radiative rates.

The parameters of the atmospheric grid are displayed in Table 1. The temperature and gravity ranges were determined by the limitations of the OSMARCS code. We are aware that some of the combinations of fundamental parameters are unlikely to correspond to any observed stars. All models were calculated with a Gaussian microturbu-

lent velocity of  $2.0 \text{ km s}^{-1}$ , this was also used in the subsequent line calculations.

The relative elemental abundances assumed for the atmospheres and for the background opacities in the non-LTE calculations are the solar abundances of Anders & Grevesse (1989). The exception is iron, for which we use the meteoritic abundance of 7.51 which is close to what analyses of Fe II lines give (e.g. Holweger et al. 1990, Biémont et al. 1991).

### 2.3. Model atom

Our B I model atom is the one compiled by Kiselman (1994) with minor refinements. It has 30 bound levels and one continuum level and features 114 line transitions. The 30 photoionisation transitions are treated as fixed rates,

**Table 1.** Fundamental parameters of the atmospheric grid

$T_{\text{eff}}$ [K]	= 5000, 5500, 6000, 6500, 7000, 7500
$\lg g$ [cgs]	= 2.00, 3.50, 4.00, 4.50
[Fe/H]	= 0.00, -1.00, -2.00, -3.00
$\xi_t$ [km s <sup>-1</sup> ]	= 2.00

calculated from the radiation field data from the model atmospheres. Photoionisation cross sections,  $f$ -values, collisional cross sections for transitions between the lower levels are theoretical data of considerable accuracy. For the lines of observational interest, we use the laboratory  $f$ -values of Johansson et al. (1993).

#### 2.4. Non-LTE code

We use the operator perturbation technique of Scharmer & Carlsson (1985) as coded in the program MULTI by Carlsson (1986). We employ MULTI version 2.2, in which line blanketing is taken into account in the photoionisation, the treatment of background opacities is improved and the many-level treatment is speeded up by using the local operator of Olson et al. (1986). This version also allows the inclusion of spectral lines in the background opacities for the line transitions treated in detail, as described in the following section.

#### 2.5. The problem of background lines

Kiselman (1994) did not include the effect of other lines blending with the B I resonance lines – the “background” opacities were just the continuous ones. The effect of such blending can be expected to be a moderation of the pumping effect that causes the departures from LTE. This will tend to decrease the positive non-LTE abundance corrections.

A full non-LTE treatment of blended lines of different atomic species is however a formidable task. In our calculations, the “background” lines are assumed to be formed in LTE and in pure absorption. (See, however, our discussion in section 4.3.2.)

It is currently not possible to assemble detailed line lists for the ultraviolet spectral regions of all the B I resonance lines. Our treatment of blending is schematic for the shortest-wavelength lines but gets more detailed towards longer wavelengths:

- The shortest-wavelength resonance lines are treated in the same way as the photoionisations, i.e. the transitions are considered to be fixed, with radiation fields computed by the atmospheric code, thus including the effect of line blanketing in an averaged way.

- For the doublet at 185 nm, background lines from the Kurucz data set are introduced, but without any observational checks on the result.
- For the region of the 209 nm doublet, a preliminary line list was kindly provided by Dr. B. Edvardsson. The resulting synthetic solar spectrum looked satisfying when compared to an uncalibrated spectrum from the Solar Maximum Mission satellite that was kindly made available by Pål Brekke.
- The background lines for the 250 nm doublet are those used in the spectrum synthesis of Duncan et al. (1992). Some new lines from the Kurucz data set were introduced to approximately fit the Procyon spectrum displayed by Lemke et al. (1993). (See the spectral region between 2498.0 Å and 2498.3 Å (air) in their Fig. 2.) The Fe II line at 2497.820 Å (air) was removed from the Duncan et al. list.

The calculation of the Boltzmann-Saha populations needed for the background line opacities is handled by the continuous-opacity package. This means that certain simplifications have to be made, for example, some elements have to be treated as others of similar ionisation potential: Ti and V as Cr, Mn and Co as Fe.

Note that it is not our aim to produce detailed synthetic spectra that can be directly compared with observations, but rather to study the departures from LTE and to acquire differential abundance corrections. The resulting spectra are, however, illustrative, and some are displayed in Figs. 1 and 2.

#### 2.6. The grid

The results presented here come from running the program for the atmospheric grid and 21 boron abundances (−1.5, −1.2, −0.9, ..., 4.2, 4.5) plus effectively zero boron abundance. For diagnostic purposes, runs with boron abundances 0.0 and 2.6 were made, for which the full computation results were saved for the lines of observational interest, including radiation-field data. All calculations were made with and without the background lines. The results from both these data sets are discussed in the following. For the sake of understanding the line-formation circumstances, we will first look at the results without background lines and view the adding of the lines as a perturbation of this case. But it is the results from the computations with background lines that will be used for the final recommended abundance corrections.

### 3. Nature of LTE departures

#### 3.1. Background

The departures from LTE that Kiselman (1994) found for the metal-poor atmosphere with low boron abundance can be described as follows.

The source function of the resonance doublets is well described by a two-level approximation, where radiative

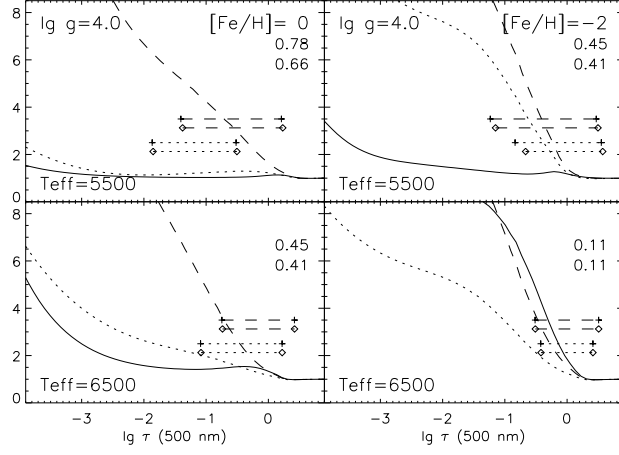


**Fig. 3.** Departure coefficients,  $A_B = 0.0$ , no background lines. Solid curve: depletion coefficient of neutral boron  $d_0 = N^*(B1)/N(B1)$ . Dotted curve:  $S^l/B_\nu$  for B1250 nm. Dashed curve:  $S^l/B_\nu$  for B1209 nm. Crosses show where the total optical depth in the line centre equals 1/3 and 3 (styles of connecting lines identify spectral lines as before), diamonds show the same thing for the continuum. Floating-point numbers give the departures from LTE in equivalent widths:  $W/W^*$  for 250 nm (upper numbers) and for 209 nm (lower numbers)

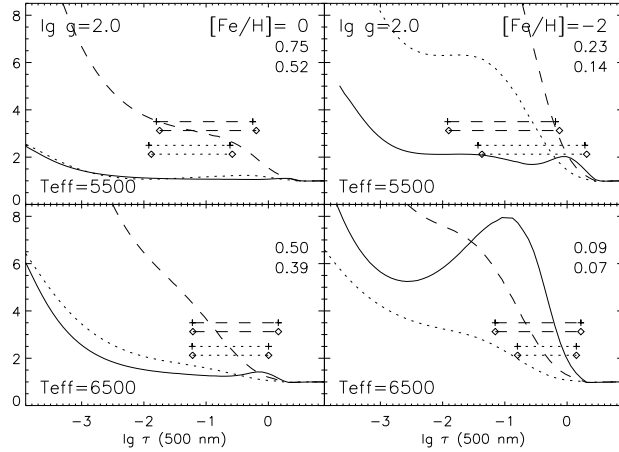


**Fig. 4.** As Fig. 3, for lower-gravity atmospheres

excitations and deexcitations dominate over collisional processes. The hot, non-local, ultraviolet radiation field causes an optical-pumping effect where the excitation balance is shifted upwards relative to LTE so that  $S^l > B_\nu$ .

The line opacities are set by the ionisation balance which departs from the Saha equilibrium in that neutral boron is depleted – overionisation. The pumping in the resonance lines causes this because the radiation fields in the ionisation edges of the excited levels are so much richer than at the ground-state ionisation edge. Furthermore, these radiation fields are stronger than the local Planckian value.

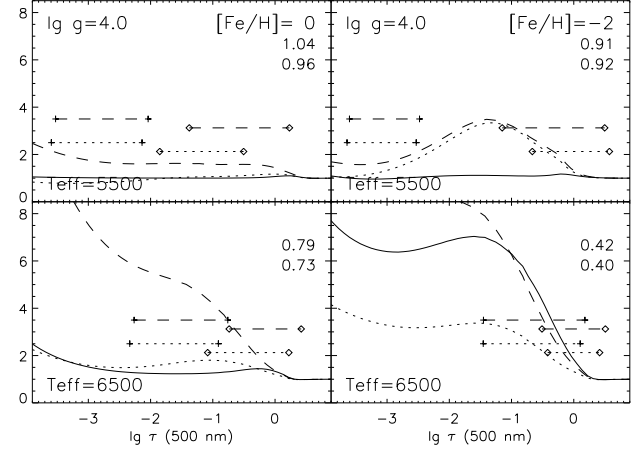


**Fig. 5.** Departure coefficients,  $A_B = 2.6$ . Designations and symbols as in Fig. 3

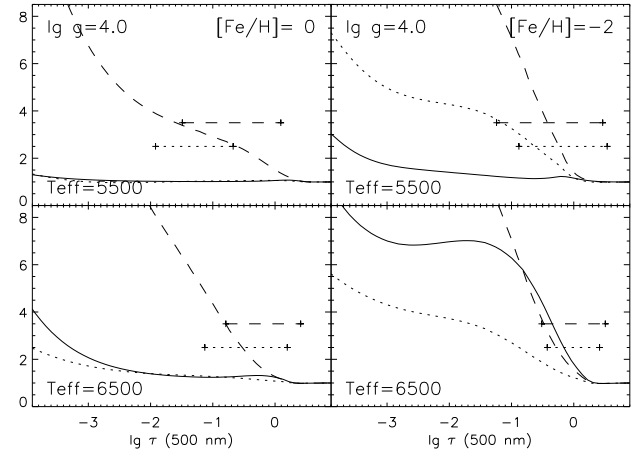


**Fig. 6.** Departure coefficients,  $A_B = 0.0$ , with background lines. Designations and symbols as in Fig. 3

The pumping and the overionisation will both make absorption lines weaker than in LTE, leading to underestimations of the boron abundance when LTE is assumed.

### 3.2. The line source function

We calculate the two-level line source function

$$S_2^l = (1 - \varepsilon) \int \phi_\nu J_\nu d\nu + \varepsilon B_\nu$$

where

$$\varepsilon = \frac{C_{ul}}{C_{ul} + A_{ul}}$$

measures the destruction probability of line photons (stimulated emission neglected). The ratio  $S^l/S_2^l$  was then studied as a measure of how good the two-level approximation for each atmosphere and boron abundance in the grid. It turned out that this ratio falls very close to 1

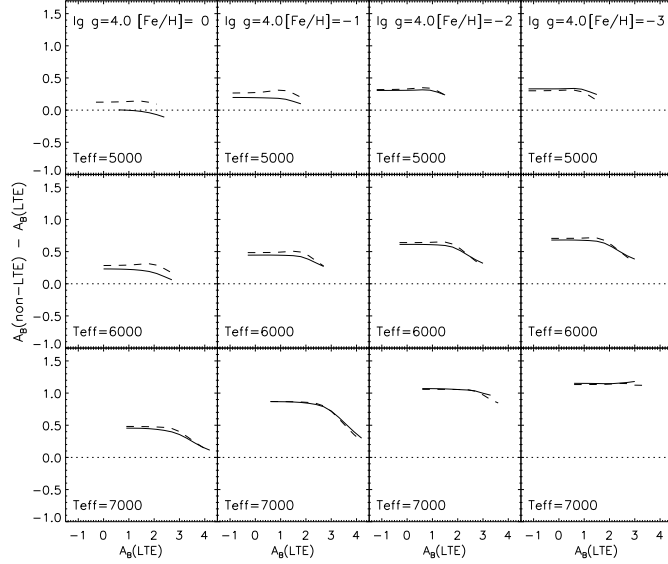


**Fig. 7.** Non-LTE abundance corrections, no background lines. Solid curve: B I 250 nm. Dashed curve: B I 209 nm

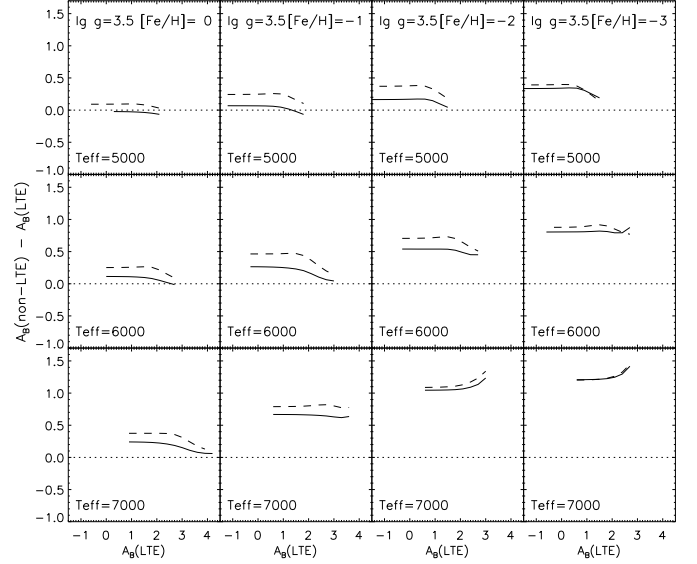


**Fig. 9.** Non-LTE abundance corrections, lines included in background opacities. Solid curve: B I 250 nm. Dashed curve: B I 209 nm

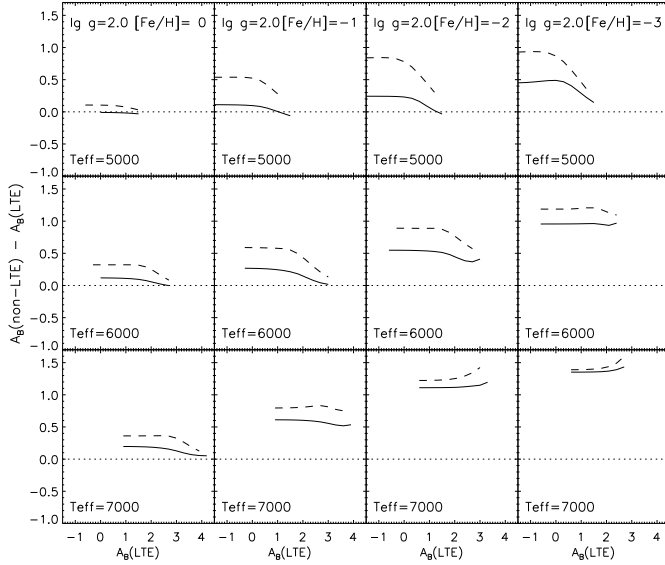


**Fig. 8.** Non-LTE abundance corrections, lines included in background opacities. Solid curve: B I 250 nm. Dashed curve: B I 209 nm

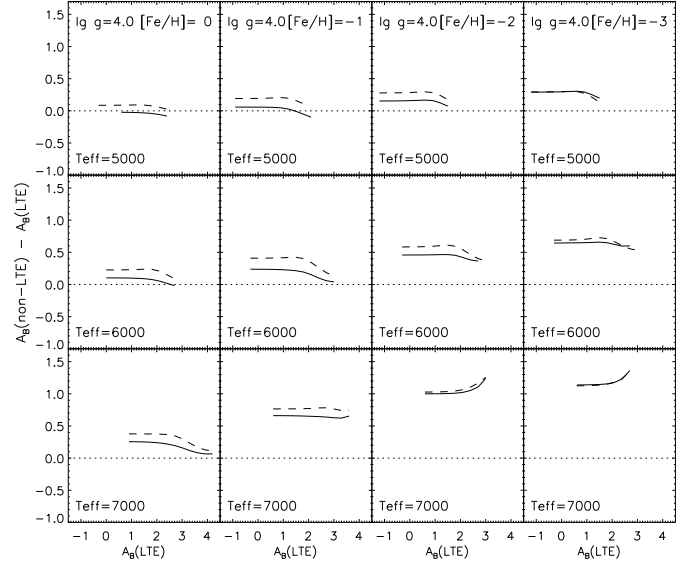


**Fig. 10.** Non-LTE abundance corrections, lines included in background opacities. Solid curve: B I 250 nm. Dashed curve: B I 209 nm

for the largest part of the grid, both with and without background lines, the exceptions are mainly for the cooler stars in the case including background lines, where the ratio goes down to  $S^I/S_2^I = 0.6$  for some models with low B abundance. This is because the line source functions for the two doublet components are forced to be equal by the strong coupling between their lower levels, while  $\int \phi_\nu J_\nu d\nu$  is quite different for the two components due to the different strength of the background lines. We consider the two-level picture adequate for discussing the departures

from LTE over the entire grid. This means that much of the discussion of Kiselman (1994) is valid.

Over most of the grid, the B I resonance lines experience pumping from the hot, non-local, radiation field. The pumping effect decreases as the boron lines grow stronger.

### 3.3. Overionisation

The relative overionisation at a given optical depth increases towards higher temperatures, lower metallicities,

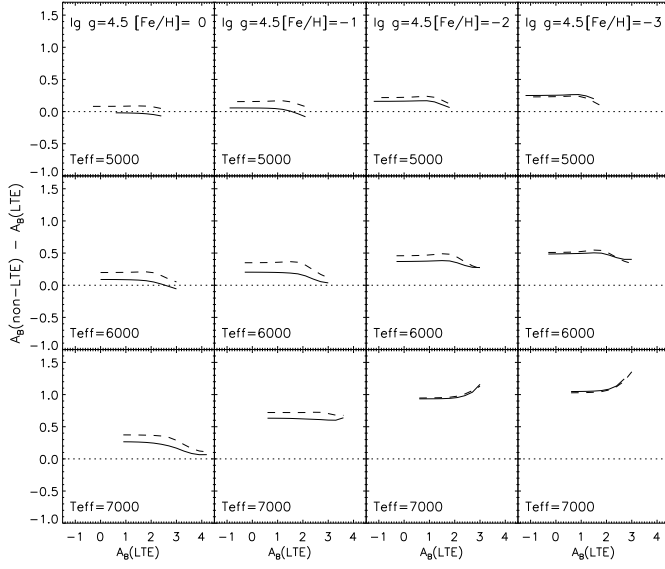


**Fig. 11.** Non-LTE abundance corrections, lines included in background opacities. Solid curve: B I 250 nm. Dashed curve: B I 209 nm

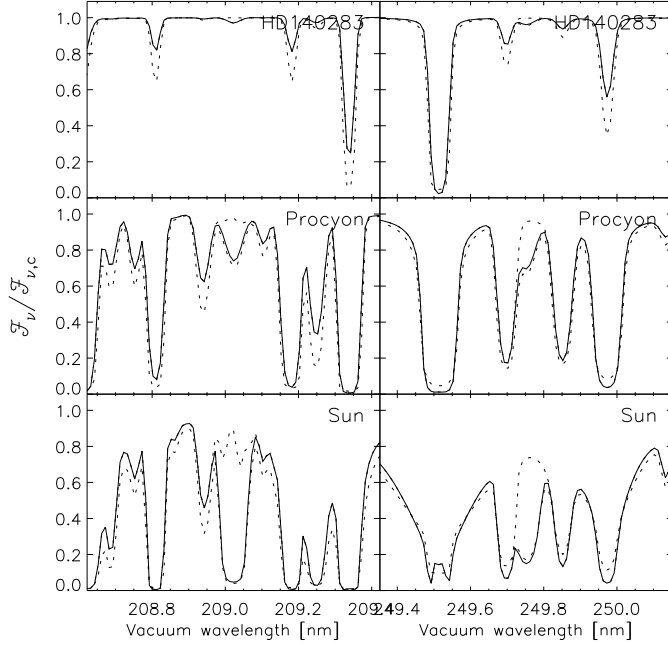


**Fig. 12.** Spectra for three stellar models computed with the background lines in pure absorption (dotted curve) and with a scattering part (solid curve). The boron abundances are  $-0.20$  (HD142083),  $1.90$  (Procyon),  $2.60$  (Sun), and, for the scattering case also zero boron abundance (dotted curve). The normalisation is the same as in Figs. 1 and 2. We stress again that what is showed here is not fits to observed spectra but the results when our methods and line lists are applied to our atmospheric models representing the three stars

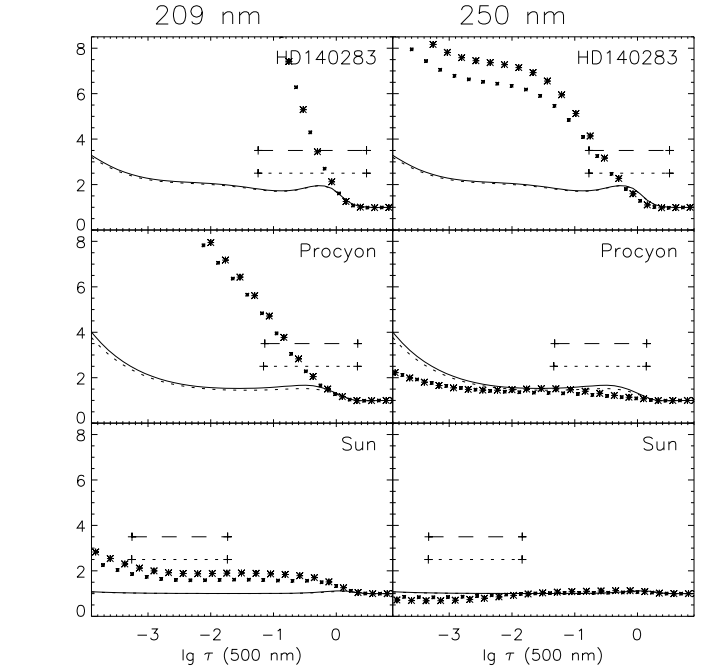


**Fig. 13.** Departure coefficients for three stellar models, parameters as in Fig. 12. The lines show  $d_0 = N^*(\text{B I})/N(\text{B I})$ , dotted for pure-absorption background lines, solid for scattering contribution. Stars show  $S^l/B_\nu$  for the line indicated at top. Small stars: pure-absorption background lines. Big stars: scattering contribution. Crosses show where the total optical depth in the line centre equals  $1/3$  and  $3$ , line styles identify background-line treatment as for  $d_0$

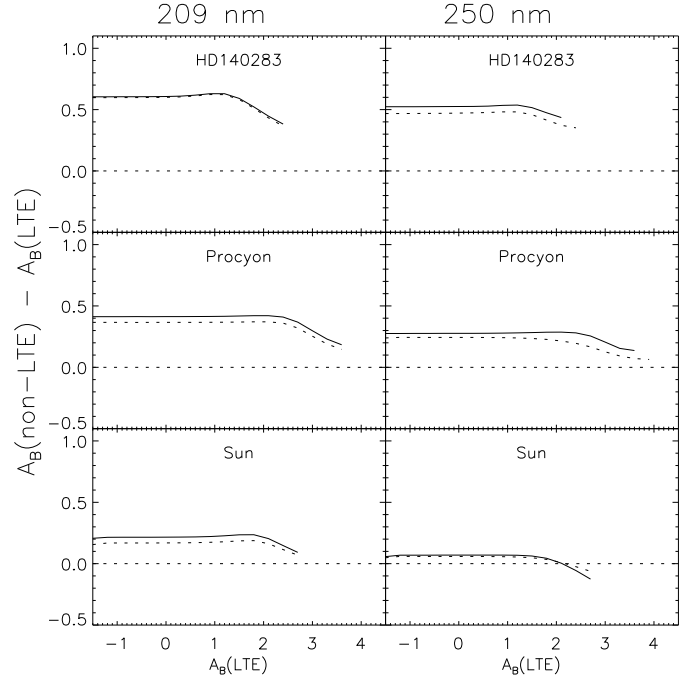


**Fig. 14.** Abundance corrections for the three stellar models. Dotted curves for pure-absorption background lines, solid curves for background with scattering

**Table 2.** Computer routines and data files available via anonymous ftp

Internet adress:	ftp.astro.uio.no
Directory:	pub/boron
Data files:	adiffb0_lte.dat, adiffb1_lte.dat
FORTTRAN interpolation routine:	corrb_nlte.f
IDL interpolation routine:	corrb_nlte.pro

**Table 3.** Non-LTE abundance correction for three specific stellar models calculated with and without a scattering contribution in the background-line opacities

Stellar model	HD140283	Procyon	Sun
$T_{\text{eff}}$ [K]	5680	6700	5780
$\lg g$ [cgs]	3.50	4.03	4.44
[Fe/H]	-2.64	-0.04	0.00
$\xi_t$ [km s $^{-1}$ ]	1.5	2.5	1.15
$A_B$ LTE	-0.20	1.90	2.60
B I 209 nm			
$\Delta A_B$ no scattering	+0.60	+0.37	+0.08
$\Delta A_B$ scattering	+0.61	+0.42	+0.11
B I 250 nm			
$\Delta A_B$ no scattering	+0.47	+0.22	-0.05
$\Delta A_B$ scattering	+0.52	+0.29	-0.10

and lower surface gravities. See Figs. 3 and 4, where the overionisation is shown (solid curve) as the depletion factor of neutral boron relative to the Saha number density:  $d_0 = N^*(\text{B I})/N(\text{B I})$ . The increase towards higher temperatures is largely due to the shift in the Saha equilibrium – the relative impact of the overionisation on the B I abundance becomes greater as boron becomes increasingly ionised.

When the B I lines become strong, the pumping effect weakens leading to less overionisation, as can be seen when comparing Figs. 3 and 6. The pumping-induced overionisation eventually turns into its opposite – the “photon suction” described by Bruls et al. (1992) for Na I and K sc i – which actually causes a marginal underionisation (overabundance of neutral boron) in the coldest, metal-rich, atmospheres of high boron abundances.

#### 3.4. Impact of background lines

The introduction of background lines should decrease the optical pumping effect simply by decreasing the local mean intensity at the line frequency. This is also seen, compare Fig. 3 with Fig. 6.

## 4. Non-LTE abundance corrections

### 4.1. Definitions

We will here present non-LTE corrections that can be used to improve LTE abundance estimates. We give such corrections rather than, e.g., presenting non-LTE curves of growth because corrections are less model-dependent, and because line blending makes it difficult to unambiguously compute or measure equivalent widths needed for a curve of growth. The ordinary procedure to get such abundance corrections is to calculate both LTE and non-LTE equivalent widths for a range of abundances. The two resulting curves of growth are then used to interpolate the LTE and the non-LTE abundances implied by a certain equivalent width. The non-LTE abundance corrections can be tabulated as functions of LTE abundance or line strength and atmospheric parameters.

This procedure is straightforward when the background continuum of the line that is studied varies little over the line width. But when we introduce lines in the background opacities, equivalent widths can be defined in several ways which will give somewhat different results when curves of growth are compared. We choose here to use a definition that essentially measures the area contained between the line and the background flux in a plot that is normalised in the way of Figs. 1 and 2. We believe this to be the measure that corresponds best with the result an abundance analyst gets when fitting synthetic spectra to observations (Kiselman & Carlsson 1995).

In practice, we use the equivalent widths as they are output from the program, their numerical values thus including a dominating contribution from the background lines. For numerical reasons, we subtract the equivalent-width value from a run with zero boron abundance. Care must also be taken to ensure that the background spectrum is numerically identical in all results, otherwise problems will arise when the boron lines are very weak.

### 4.2. Results

The plots of Figs. 7-11 display the non-LTE abundance corrections as functions of LTE abundances for some cross sections of the grid. The range in LTE abundance for each plot is naturally limited by the boron abundance grid. We have also introduced limits to ensure that the lines are strong enough to be of any observational interest and that they are weak enough for our modelling to be relevant. The lower limit on line strength is  $W < 0.1 \text{ pm} = 1 \text{ mÅ}$  (from the case without background lines). The upper limit is set to assure that the line centre is optically thin at the uppermost point of the model atmosphere ( $\lg \tau < -0.1$ ).

The curves in the plots are generally flat, illustrating that the departures from LTE are set by the background radiation fields as long as the B I lines are weak. When the resonance lines become strong enough to influence their own radiation fields, the pumping effects decreases, and so does the overionisation. This leads to the downturn in the



abundance correction curves seen in many of the plots. In some cases, for the exotic parameter combination of hot, very metal-poor stars with high boron abundance, there is a hint of an upturn instead. The boron lines are here still rather weak (cf. Figs. 1 and 2), and we interpret the upturn as a result of the lines being formed at greater heights in the atmosphere where the relative overionisation is larger.

Figure 7 displays the corrections without background lines for  $\lg g = 4.0$ . Compare this with Fig. 9 to see the importance of the background lines.

The corrections calculated for the entire grid are available, together with interpolation routines, via ftp from <ftp.astro.uio.no>, directory pub/boron. The routines and formats are similar to those presented by Carlsson et al. (1994) for Li abundance corrections. More details are given in Table 2.

For quick reference, we also present numerical values for the corrections (B I 250 nm) over a part of the grid representing solar-like stars in Table 5.

### 4.3. Uncertainties

#### 4.3.1. General

The model-atom uncertainties are discussed by Kiselman (1994) who concludes that they are not likely to be the most important cause of errors.

Our corrections are model dependent and should really only be applied to LTE results acquired with the same atmospheric models. Model-atmosphere errors and differences, within the plane-parallel paradigm, will, however, probably influence the non-LTE corrections only to second order. Effects caused by granulation and other kinds of photospheric inhomogeneity is probably a matter of greater concern. (And would be so even if the lines were formed in perfect LTE.)

The 250 nm doublet is approaching optical thickness in the uppermost point of our solar-like atmospheric models with high boron abundance when background lines are included. The modelling is then not very realistic, especially since the lines should be affected by a chromospheric temperature rise. Everything seems to imply, however, that departures from LTE will be small for stars similar to the Sun.

#### 4.3.2. Background lines

Errors in the line lists and inadequacies in our treatment of background lines influence the results in two ways. First, errors in oscillator strengths and non-LTE effects can cause the background opacities to be erroneous. This could in principle be mended by detailed fitting to observed spectra. (Something which would be needed anyhow to allow for the detailed abundance pattern of individual stars.) Second, errors in the background source function are introduced by treating the line opacities as pure absorption.

This will tend to thermalise the transitions involved. The effect of photon escape, which would lead to  $S^l < B_\nu$  for strong lines is expected to be suppressed leading to a line source function of the boron line that is too close to the LTE value. Abundance corrections will then be close to zero instead of negative (if overionisation is negligible).

We have investigated the latter effect by introducing a scattering part in the background line opacities via a line-photon destruction probability  $\varepsilon = \frac{C_{ul}}{C_{ul} + A_{ul}}$  that is calculated using Van Regemorter's (1962) approximation for the collisional rate. Thus the absorption fraction of the line opacity is

$$\frac{\kappa_l}{\kappa_l + \sigma_l} = \varepsilon$$

and the scattering fraction

$$\frac{\sigma_l}{\kappa_l + \sigma_l} = 1 - \varepsilon.$$

This was done for atmospheric models representing the Sun, Procyon and the halo star HD140283 (the same models as in Kiselman 1994) and the same range of B abundances as in the main grid. The results are illustrated in Figs. 12, 13, 14, and Table 3.

Figure 12 compares the appearance of spectra as computed with (solid curve) and without (dotted curve) scattering in background lines.

The relevant departure coefficients are shown in Fig. 13 in the same way as in Figs. 3–6. The most significant difference is in the line source function of the 250 nm line.

Figure 14 displays non-LTE abundance corrections as function of derived LTE abundance (in a similar way as Figs. 7–11) for the cases with (solid curves) and without (dashed curves) scattering in background lines. The effect of introducing the background scattering is to increase the magnitude of the abundance corrections, regardless whether these are positive or negative. (Note the crossing of the curves at the zero level for the solar 250 nm case.) This is expected since we decrease the photon-destruction probability and thus increase the effective photon path length – the non-local nature of the radiation field is enhanced. The differences in abundance corrections are, however, small – never more than 0.1 dex.

We conclude that a refined treatment of background lines may make the non-LTE corrections slightly greater. We note, however, that any such refinement would need adjustments of the line lists in order for the treatment to be consistent.

## 5. Impact on existing observations

Table 4 features LTE boron abundances from the literature and the abundances after the non-LTE corrections from this paper have been applied. The non-LTE corrections have been interpolated from the grid, which explains the small differences for the three stars of Table 3. The

**Table 4.** Reanalysis of literature data. The sources for the LTE boron abundances and atmospheric parameters are: *a)* Edvardsson et al. 1994, *b)* Duncan et al. 1992, *c)* Lemke et al. 1993, *d)* Kohl et al. 1977. The non-LTE abundances in column N were calculated without background lines. In column A background lines were included (these are our recommended abundances). The A value for the Sun is given although the line core is optically thick at the uppermost atmospheric point at this abundance

Star	$T_{\text{eff}}$ [K]	$\lg g$ [cgs]	[Fe/H]	$A_{\text{B}}$ LTE	$A_{\text{B}}$ N	$A_{\text{B}}$ A
HD140283 <sup>a</sup>	5680	3.50	-2.64	-0.20	0.39	0.29
HD19445 <sup>b</sup>	5880	4.40	-2.15	0.40	0.87	0.76
HD201891 <sup>b</sup>	5870	4.50	-1.06	1.70	2.06	1.86
$\theta$ UMa <sup>c</sup>	6380	4.09	-0.14	2.30	2.59	2.43
Procyon <sup>c</sup>	6700	4.03	-0.04	1.90	2.28	2.10
$\iota$ Peg <sup>c</sup>	6750	4.35	-0.04	2.40	2.77	2.58
Sun <sup>d</sup>	5780	4.44	0.00	2.60	2.64	2.55

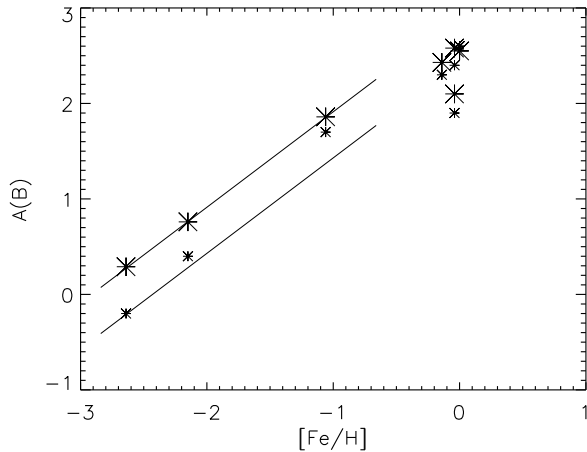


**Fig. 15.** Boron abundances for solar-type stars plotted as a function of metallicity. Data from Table 4, small stars are LTE abundances. Two lines with B/Fe = constant are drawn for comparison

abundance data is displayed in Fig. 15 as a plot of boron abundance against metallicity for the stars of Table 4.

The inclusion of background lines moderates somewhat the magnitude of the non-LTE effects for HD140283 and Procyon found by Kiselman (1994). The change in abundance for the extreme halo star HD140283 is small, however, and the conclusions of Edvardsson et al. (1994) regarding the boron/beryllium ratio are unaffected. For Procyon, it seems that the new results reconfirm the general conclusion of Lemke et al. (1993) that this star really is somewhat boron depleted relative to the Sun.

The new result for the Sun indicates a slightly lower boron abundance than before. Note, however, that we have adopted the rather uncertain photospheric LTE abundance of  $2.60 \pm 0.3$  that was derived by Kohl et al. (1978). The meteoritic abundance is  $2.88 \pm 0.04$  (Anders & Grevesse 1989) and may perhaps be more realistic.

It is interesting to note that, for the three metal-poor stars, the non-LTE corrected [B/Fe] is close to constant, in contrast to the LTE results, see Fig. 15.

## 6. Conclusions

We have presented a study of departures from LTE for neutral boron in a grid of cool stellar atmospheric models. The processes responsible for these departures over the grid are essentially the same as those described by Kiselman (1994). The non-LTE abundance corrections are generally greatest for hot, metal-poor, and low-gravity stars, i.e. they become more important as the B I lines get weaker for a fixed B abundance. LTE abundances based on B I lines should always be corrected for these effects. We have presented such corrections for cool stars and made them available in computer-readable form.

*Acknowledgements.* We thank Bengt Edvardsson for help with line lists and valuable comments on the manuscript. Thanks are also due to Pål Brekke for providing the solar UV spectrum.

## References

- Anders E., Grevesse N., 1989, *Geochim. Cosmochim. Acta*, 53, 197
- Bell R.A., Paltoglou G., Tripicco M.J., 1994, *MNRAS*, 268, 771
- Bell R.A., Tripicco M.J., *Synthetic Spectra, Synthetic colours and line lists*. In: Adelman S.J., Wiese W.L. (eds.), *Astrophysical Applications of Powerful New Databases*, ASP Conference Series, Vol. 78, p.367
- Biémont E., Baudoux M., Kurucz R.L., Ansbacher W., Pinnington E.H., 1991, *A&A*, 249, 539
- Bruls J.H.M.J., Rutten R.J., Shchukina N.G., 1992, *A&A*, 265, 237
- Buser R., Kurucz R.L., 1992, *A&A*, 264, 557
- Carlsson M., 1986, *Uppsala Astronomical Observatory Report No. 33*
- Carlsson M., Rutten R.J., Bruls J.H.M.J., Shchukina N.G., 1994, *A&A*, 288, 860
- Duncan D.K., Lambert D.L., Lemke M., 1992, *ApJ*, 401, 584
- Duncan D.K., Peterson R.C., Thorburn J.A., Pinsonneault M.H., Deliyannis C.P., 1995, *Boron in the Hyades giants*. In: Crane P. (ed.), *The Light Elements Abundances*, Springer, p. 425
- Edvardsson B., Andersen J., Gustafsson B., et al., 1993, *A&A*, 275, 101
- Edvardsson B., Gustafsson B., Johansson S.G., et al., 1994, *A&A*, 290, 176
- Gustafsson B., Bell R.A., Eriksson K., Nordlund Å., 1975, *A&A*, 42, 407
- Gustafsson B., 1995, *Opacity incompleteness and atmospheres of late-type stars*. In: Adelman S.J., Wiese W.L. (eds.), *As-*

trophysical Applications of Powerful New Databases, ASP Conference Series, Vol. 78, p.347  
 Holweger H., Heise C., Kock M., 1990, A&A, 232, 510  
 Johansson S.G., Litzén U., Kasten J., Kock M., 1993, ApJ, 403, L25  
 Kohl J.L., Parkinson W.H., Withbroe G.L., 1977, ApJ, 212, L101  
 Kiselman D., 1994, A&A, 286, 169  
 Kiselman D., Carlsson M., 1995, Non-LTE effects on Be and B abundance determinations in cool stars. In: Crane P. (ed.), The Light Elements Abundances, Springer, p.372  
 Kurucz R.L., 1991, New opacity calculations. In: Crivellari L. (ed.), Stellar atmospheres: Beyond Classical Models, Kluwer, p.441  
 Lemke M., Lambert D.L., Edvardsson B., 1993, PASP, 105, 468  
 Olson G.L., Auer L.H., Buchler J.R., 1986, JQSRT, 35, 431  
 Scharmer G.B., Carlsson, M., 1985, J.Comput.Phys. 59, 56  
 Van Regemorter H., 1962, ApJ, 136, 906

**Table 5.** Numerical non-LTE abundance corrections (in dex) for B I 250 nm for part of the atmosphere grid (computed with background lines). The corrections should be added to LTE abundances. Gaps in the tables mean that the line is too weak or too strong according to the criteria described in section 4.2, or simply that the (LTE) abundance falls outside the abundance range

$T_{\text{eff}} / \lg g / [\text{Fe}/\text{H}]$ [K]/[cgs]/	$A_{\text{B}}(\text{LTE})$				
	0.00	0.90	1.50	2.10	2.40
5000/2.00/ 0.00	−0.01	−0.02	−0.03		
5000/2.00/−1.00	+0.10	+0.02	−0.06		
5000/2.00/−2.00	+0.23	+0.09	−0.03		
5000/2.00/−3.00	+0.49	+0.32	+0.15		
5000/3.50/ 0.00		−0.03	−0.04	−0.07	
5000/3.50/−1.00	+0.07	+0.05	−0.02		
5000/3.50/−2.00	+0.17	+0.15	+0.04		
5000/3.50/−3.00	+0.34	+0.31	+0.19		
5000/4.50/ 0.00		−0.02	−0.03	−0.05	−0.07
5000/4.50/−1.00	+0.06	+0.05	+0.01	−0.08	
5000/4.50/−2.00	+0.16	+0.17	+0.11		
5000/4.50/−3.00	+0.25	+0.26	+0.20		
6000/2.00/ 0.00	+0.12	+0.11	+0.09	+0.05	+0.02
6000/2.00/−1.00	+0.27	+0.25	+0.21	+0.13	+0.08
6000/2.00/−2.00	+0.55	+0.54	+0.51	+0.43	+0.38
6000/2.00/−3.00	+0.96	+0.96	+0.96	+0.93	+0.97
6000/3.50/ 0.00	+0.11	+0.11	+0.10	+0.05	+0.02
6000/3.50/−1.00	+0.26	+0.25	+0.23	+0.16	+0.10
6000/3.50/−2.00	+0.54	+0.54	+0.54	+0.49	+0.45
6000/3.50/−3.00	+0.81	+0.81	+0.82	+0.79	+0.79
6000/4.50/ 0.00	+0.09	+0.09	+0.08	+0.05	+0.02
6000/4.50/−1.00	+0.20	+0.20	+0.19	+0.15	+0.10
6000/4.50/−2.00	+0.37	+0.37	+0.38	+0.35	+0.31
6000/4.50/−3.00	+0.49	+0.49	+0.50	+0.47	+0.43
7000/2.00/ 0.00		+0.20	+0.19	+0.18	+0.17
7000/2.00/−1.00		+0.61	+0.61	+0.60	+0.59
7000/2.00/−2.00		+1.11	+1.11	+1.12	+1.13
7000/2.00/−3.00		+1.35	+1.36	+1.37	+1.39
7000/3.50/ 0.00		+0.24	+0.24	+0.22	+0.21
7000/3.50/−1.00		+0.67	+0.67	+0.66	+0.65
7000/3.50/−2.00		+1.05	+1.05	+1.07	+1.09
7000/3.50/−3.00		+1.21	+1.22	+1.25	+1.30
7000/4.50/ 0.00		+0.27	+0.26	+0.25	+0.23
7000/4.50/−1.00		+0.63	+0.63	+0.62	+0.62
7000/4.50/−2.00		+0.93	+0.94	+0.95	+0.98
7000/4.50/−3.00		+1.05	+1.05	+1.08	+1.13